Electronic Supplementary Material (ESI) for CrystEngComm.
This journal is © The Royal Society of Chemistry 2021

# Supporting Information

## Influence of linker substitution on fluorescence responsive sensing of isostructural coordination polymers: visual turn-on, ratiometric, and turn-off sensing in water

Po-Min Chuang, Yun-Wen Huang, Yu-Lin Liu, and Jing-Yun Wu*

Department of Applied Chemistry, National Chi Nan University, Nantou 545, Taiwan. E-mail: jyunwu@ncnu.edu.tw

## Experimental section

### Materials and instruments

Chemicals were commercially obtained and used without further purification. Ligand Cz-3,6-bpy was prepared according to the literature report.[S1] $^1$H NMR spectra were measured using a Bruker AMX-300 Solution-NMR spectrometer. Chemical shifts are reported in parts per million (ppm) with reference to the residual protons of the deuterated solvent, and coupling constants are reported in hertz (Hz). High resolution fast atom bombardment mass spectra (HR FAB-MS) were performed using a JEOL JMS-700 double focusing mass spectrometer with a resolution of 8000 (5% valley definition); NBA (3-nitrobenzyl alcohol) was chosen as matrix. Infrared (IR) spectra were carried out using a Perkin-Elmer Frontier Fourier transform infrared spectrometerwith attenuated total reflection (ATR) technique; abbreviations used for the IR bands are br = broad, s = strong, m = medium, w = weak. UV-vis absorption spectra were measured using a JASCO V-750 UV/VIS spectrophotometer. Room temperature fluorescence spectra were measured using a Hitachi F7000 fluorescence spectrophotometer equipped with a 150 W xenon lamp as an excitation source. X-ray powder diffraction (XRPD) patterns were measured using a Shimadzu XRD-7000 diffractometer equipped with a graphite monochromatized Cu sealed tube with K$\alpha$ radiation ($\lambda$ = 1.5406 Å) at 30 kV and 30 mA. Thermogravimetric (TG) analyses were conducted using a Thermo Cahn VersaTherm HS TG analyzer with a flux nitrogen atmosphere and a heating rate of 5 °C min$^{-1}$. CHN microanalyses were conducted using an Elementar Vario EL III analytical instrument. Ultrasonic agitation of suspensions was performed using a Qsonica Q125 instrument. Inductively coupled plasma optical emission spectrometry (ICP-OES) analyses were carried out using an Agilent 5100 ICP-OES instrument. X-ray photoelectron spectroscopy (XPS) analyses were conducted on a Thermo Scientific ESCALAB 250 surface analysis system with a monochromatic Al Kα source (beam energy = 1486.7 eV) and a spherical sector analyzer. The binding energy was referenced to adventitious C1*s* peak at 284.8 eV.

### Synthesis of 3,6-dibromo-9-*n*-propyl-9*H*-carbazole

In a three neck, round-bottomed flask, 3,6-dibromo-9*H*-carbazole (1.625 g, 5.0 mmol), 1-bromopropane (1.845 g, 15.0 mmol), and toluene (30 mL) were sequentially added. Then an aqueous solution (20 mL) of tetra-*n*-butylammonium bromide (TBAB, 161 mg, 0.50 mmol) and KOH (672 mg, 12.0 mmol) was added. The mixture was refluxed with stirring at 110 °C for 24 h. After the reaction mixture cooling to room temperature, deionization water (20 mL) and dichloromethane (40 mL) were added for extraction. The organic extracts were collected and dried over anhydrous magnesium sulfate. Then, *n*-hexane (50 mL) was added. After the solution was filtered off, the solvent was removed under reduced pressure. The crude products were purified to be white precipitates by recrystallization twice using ethanol as solvent. Yield: 89% (1.615 g, 4.45 mmol). $^1$H NMR (300 MHz, DMSO-$d_6$, ppm): $\delta$ 8.47 (s, *2*H), 7.65-7.57 (m, 4H), 4.36 (t, *J* = 6.9 Hz, 2H), 1.76 (h, *J* = 6.6 Hz, 2H), 0.83 (t, *J* = 4.9 Hz, 3H). HR-MS (FAB$^+$): *m/z* 364.9411 [M]$^+$ (364.9411 for $C_{15}H_{13}N(^{79}Br)_2$). IR (ATR, cm$^{-1}$): 3067w, 2967m, 2927w, 2875w, 1856w, 1718w, 1585m, 1466s, 1433s, 1380m, 1347m, 1288s, 1215s, 1149m, 1056m, 1016m, 864m, 831s, 792s, 646m, 560m. Anal. Calcd for $C_{15}H_{13}NBr_2$: C, 49.08; H, 3.57; N, 3.82%. Found: C, 49.33; H, 3.39; N, 3.84%. UV-vis (DMF, nm): $\lambda$

335sh ($\varepsilon$ = 22200 L mol$^{-1}$ cm$^{-1}$), 347 ($\varepsilon$ = 33300 L mol$^{-1}$ cm$^{-1}$), 363 ($\varepsilon$ = 33600 L mol$^{-1}$ cm$^{-1}$).

**Synthesis of 3,6-bis(pyridin-4-yl)-9-*n*-propyl-9*H*-carbazole (Cz-Pr-3,6-bpy)**

3,6-Dibromo-9-*n*-propyl-9*H*-carbazole (1.089 g, 3.0 mmol), pyridine-4-boronic acid (886 mg, 7.2 mmol), $Pd(PPh_3)_4$ (289 mg, 0.25 mmol), and $K_2CO_3$ (997 mg, 7.2 mmol) were sequentially added into a three neck, round-bottomed flask. The flask was alternately vacuumed and purged argon atmosphere three times. A mixture of deionization water (30 mL), ethanol (30 mL), and 1,4-dioxane (90 mL) were degassed and then added. The reaction mixture was heated to 90 °C with stirring for 48 h under argon atmosphere. After the reaction mixture cooling to room temperature, deionization water (30 mL) and dichloromethane (60 mL) were added for extraction. The organic extracts were collected, filtered with Celite 545, and dried over anhydrous magnesium sulfate. After the solution was filtered off, the solvent was removed under reduced pressure. The crude product was purified by column chromatography (silica gel, ethyl acetate/tetrahydrofuran, 5:1 v/v, followed by ethanol) to give Cz-Pr-3,6-bpy as a golden-yellow precipitates. Yield: 79% (860 mg, 2.4 mmol). $^1$H NMR (300 MHz, DMSO-$d_6$, ppm): $\delta$ 8.87 (s, 2H), 8.64–8.63 (m, 4H), 7.97–7.94 (m, 2H), 7.87–7.85 (m, 4H), 7.77 (d, $J$ = 8.7 Hz, 2H), 4.45 (t, $J$ = 6.8 Hz, 2H), 1.84 (q, $J$ = 7.0 Hz, 2H), 0.88 (t, $J$ = 7.4 Hz, 3H). HR-MS (FAB$^+$): *m/z* 364.1822 $[M+H]^+$ (364.1814 for $C_{25}H_{22}N_3$). IR (ATR, cm$^{-1}$): 3027w, 2960w, 2920w, 2875w, 1592s, 1545w, 1473s, 1413w, 1380w, 1347w, 1288s, 1215s, 1129w, 1069w, 1030w, 990w, 891w, 798s, 666w, 573w. Anal. Calcd for $C_{25}H_{21}N_3$: C, 82.61; H, 5.82; N, 11.56%. Found: C, 82.35; H, 5.79; N, 11.42%. UV-vis (DMF, nm): $\lambda$ 297 ($\varepsilon$ = 35500 cm$^{-1}$ M$^{-1}$), 329 ($\varepsilon$ = 20800 cm$^{-1}$ M$^{-1}$).

**General procedures for synthesis of Zn coordination polymers 1–4**

An aqueous solution (3 mL) of $Zn(NO_3)_2{\cdot}6H_2O$ (0.050 mmol), a *N*,*N*′-dimethylformamide (DMF) solution (1 mL) of aromatic dicarboxylic acid (0.050 mmol), and a DMF solution (1 mL) of carbazole-based bispyridyl ligand (0.025 mmol) were sequentially sealed in a 23-mL Teflon-lined flask, which was then placed in a stainless steel bomb. The bomb was placed in an oven and then heated to 100 °C from room temperature in a period of 6 h. The temperature was maintained at 100 °C for 36 h or 48 h, and then cooled to 30 °C in a period of 48 h or 36 h. The resulted crystals were collected.

**$\{[Zn_2(OH)(NO_2\text{-}1,4\text{-}bdc)_{1.5}(Cz\text{-}3,6\text{-}bpy)]\cdot 2H_2O\}_n$ (1):** Golden-yellow crystals were collected in a yield of 70% based on Cz-3,6-bpy (14.3 mg, 0.0175 mmol). IR (ATR, cm$^{-1}$): 3238br, 1737m, 1598s, 1532m, 1479m, 1367s, 1288w, 1228m, 1036w, 924w, 831m, 779m, 732m, 600m. Anal. Calcd for $C_{34}H_{20.5}N_{4.5}O_{10}Zn_2{\cdot}H_4O_2$: C, 49.87; H, 3.02; N, 7.70%. Found: C, 49.90; H, 3.04; N, 7.91%.

**$\{[Zn_2(OH)(NO_2\text{-}1,4\text{-}bdc)_{1.5}(Cz\text{-}Pr\text{-}3,6\text{-}bpy)]\cdot 0.5H_2O\}_n$ (2):** Golden-yellow crystals were collected in a yield of 35% based on Cz-Pr-3,6-bpy (7.3 mg, 0.0088 mmol). IR (ATR, cm$^{-1}$): 2972w, 1591s, 1531m, 1477s, 1343s, 1289m, 1215m, 1142w, 1075m, 1041m, 934w, 833m, 800m, 699w, 605w, 518w. Anal. Calcd for $C_{37}H_{26.5}N_{4.5}O_{10}Zn_2{\cdot}HO_{0.5}$: C, 53.29; H, 3.32; N, 7.56%. Found: C, 53.24; H, 3.23; N, 7.74%.

**$\{[Zn_2(OH)(Br\text{-}1,4\text{-}bdc)_{1.5}(Cz\text{-}3,6\text{-}bpy)]\cdot H_2O\}_n$ (3):** Golden-yellow crystals were collected in a yield of 66% based on Cz-3,6-bpy (14.1 mg, 0.0165 mmol). IR (ATR, cm$^{-1}$): 3220br, 1584s, 1477m, 1370s,

1282m, 1222m, 1142w, 1075m, 1035m, 833m, 806m, 773m, 599w, 538w. Anal. Calcd for $C_{34}H_{20.5}N_3O_7Br_{1.5}Zn_2 \cdot H_2O$: C, 47.95; H, 2.66; N, 4.94%. Found: C, 47.83; H, 2.88; N, 5.24%.

**{[$Zn_2$(OH)(Br-1,4-bdc)$_{1.5}$(Cz-Pr-3,6-bpy)]·$H_2O$}$_n$ (4):** Pale-yellow crystals were collected in a yield of 18% based on Cz-Pr-3,6-bpy (4.0 mg, 0.0045 mmol). IR (ATR, $cm^{-1}$): 2972w. 1591s, 1477m, 1376s, 1282m, 1222m, 1135w, 1075m, 1035m, 833m, 800m, 766m, 612w, 511m. Anal. Calcd for $C_{37}H_{26.5}N_3O_7\ Br_{1.5}Zn_2 \cdot HO_{0.5}$: C, 50.23; H, 3.13; N, 4.75%. Found: C, 50.31; H, 3.27; N, 4.86%.

**Single-crystal X-ray structure determinations**

A Bruker D8 Venture diffractometer equipped with graphite monochromatized Mo K$\alpha$ radiation ($\lambda$ = 0.71073 Å) was used to collect the X-ray diffraction data at 150(2) K for indexing and solving structure of **1**–**4**. Direct methods with SHELXS-97 program[S2] were applied to find the initial model for structure refinement. Structural data were refined by full-matrix least-squares methods against $F^2$ using the SHELXL-2014/7,[S3] incorporated in WINGX-v2014.1[S4] crystallographic collective package. Non-hydrogen atoms were positioned from difference Fourier maps and refined with anisotropic temperature parameters, with exception of lattice water molecules in **1**–**4** and the disordered nitro group in **2**. The lattice water molecules in **2**–**4** were refined in partial site of occupancy. Hydrogen atoms bound on carbon atoms were geometrically placed and refined as riding mode, while that bound on nitrogen atoms and oxygen atoms were structurally evident in the difference Fourier map, and then fixed at calculated positions and included in the final refinement. No attempt was made to find the hydrogen atoms of lattice water molecules in **2**–**4**. All of the hydrogen atoms were refined with isotropic temperature parameters. The crystallographic data and structure refinement parameters are summarized in Table S1. CCDC 1991629−1991632 contain the supplementary crystallographic data for this paper. These data can be obtained free of charge from the Cambridge Crystallographic Data Centre via www.ccdc.cam.ac.uk/data_request/cif.

**Fluorescence sensing experiments**

The fluorescence sensing experiments were evaluated using the $H_2O$ suspensions of **1**–**4**. Crystalline solids (1 mg) were carefully ground and dispersed in $H_2O$ (3 mL), which were then ultrasonicated agitation with pulsed ultrasound for 10 min and aging for further 30 min to form uniformly stable suspensions. Aqueous solutions containing $NaNO_3$, $KNO_3$, $Mg(NO_3)_2$, $Ca(NO_3)_2$, $Mn(NO_3)_2$, $Co(NO_3)_2$, $Ni(NO_3)_2$, $Cu(NO_3)_2$, $Cd(NO_3)_2$, $AgNO_3$, $Pb(NO_3)_2$, $Fe(NO_3)_3$, $Al(NO_3)_3$, and $Cr(NO_3)_3$ for metal ion sensing experiments and NaF, KCl, KBr, KI, $KNO_3$, $Na_2SO_4$, $K_2CO_3$, $K_3PO_4$, $KClO_4$, $K_2CrO_4$, and $K_2Cr_2O_7$ for anion sensing experiments with a concentration at 0.10 M were separately prepared. These analyte aqueous solutions were directly utilized for qualitative sensing experiments and diluted to have a concentration of 0.010 M for quantitative sensing experiments. The titration experiments were performed by the addition of metal ions and anions in aqueous solutions step by step, and the luminescence emission spectra were recorded.

**Table S1.** Crystallographic data for **1**–**4**

| | **1** | **2** | **3** | **4** |
|---|---|---|---|---|
| CCDC number | 1991629 | 1991630 | 1991631 | 1991632 |
| Empirical formula | $C_{34}H_{24}N_{4.5}O_{12}Zn_2$ | $C_{37}H_{27.5}N_{4.5}O_{10.5}Zn_2$ | $C_{34}H_{22.5}Br_{1.5}N_3O_8Zn_2$ | $C_{37}H_{27.5}Br_{1.5}N_3O_{7.5}Zn_2$ |
| $M_w$ | 818.32 | 833.87 | 851.65 | 884.72 |
| Crystal system | Monoclinic | Monoclinic | Monoclinic | Monoclinic |
| Space group | *C*2/*c* | *C*2/*c* | *C*2/*c* | *C*2/*c* |
| *a* (Å) | 23.723(2) | 24.717(3) | 24.379(2) | 24.8175(17) |
| *b* (Å) | 18.8503(19) | 19.189(3) | 18.810(2) | 19.1673(17) |
| *c* (Å) | 15.0119(13) | 15.197(2) | 15.0638(13) | 15.1781(11) |
| $\beta$ (°) | 102.003(4) | 105.906(6) | 104.484(4) | 106.266(4) |
| *V* (Å$^3$) | 6566.4(11) | 6931.6(17) | 6688.4(11) | 6931.0(9) |
| *Z* | 8 | 8 | 8 | 8 |
| *T* (K) | 150(2) | 150(2) | 150(2) | 150(2) |
| λ (Å) | 0.71073 | 0.71073 | 0.71073 | 0.71073 |
| $D_{calc}$ (g cm$^{-3}$) | 1.656 | 1.598 | 1.692 | 1.696 |
| $F_{000}$ | 3324 | 3400 | 3392 | 3544 |
| $\mu$ (mm$^{-1}$) | 1.536 | 1.453 | 3.283 | 3.170 |
| $R_1$ [$I > 2\sigma(I)$][a] | 0.0565 | 0.0826 | 0.0770 | 0.0719 |
| $wR_2$ [$I > 2\sigma(I)$][a] | 0.1383 | 0.1850 | 0.1804 | 0.1665 |
| $R_1$ (all data][b] | 0.0791 | 0.1351 | 0.1176 | 0.0890 |
| $wR_2$ (all data][b] | 0.1554 | 0.2313 | 0.2069 | 0.1826 |
| GOF on $F^2$ | 1.075 | 1.133 | 1.119 | 1.067 |

[a] $R_1 = \sum\left\|F_o\right| - \left|F_c\right\| \Big/ \sum\left|F_o\right|$. [b] $wR_2 = \{\sum[w(F_o^{\,2} - F_c^{\,2})^2] \Big/ \sum[w(F_o^{\,2})^2]\}^{1/2}$.

## References


S1 Y.-W. Huang, P.-M. Chuang and J.-Y. Wu, Solvent-Induced Controllable Supramolecular Isomerism: Phase Transformation, $CO_2$ Adsorption, and Fluorescence Sensing toward $CrO_4^{2-}$, $Cr_2O_7^{2-}$, $MnO_4^-$ and $Fe^{3+}$, *Inorg. Chem.*, 2020, **59**, 9095–9107.

S2 G. M. Sheldrick, A short history of SHELX, *Acta Crystallogr., Sect. A*, 2008, **64**, 112–122.

S3 G. M. Sheldrick, Crystal structure refinement with SHELXL, *Acta Crystallogr., Sect. C*, 2015, **71**, 3–8.

S4 L. J. Farrugia, WinGX and ORTEP for Windows: an update, *J. Appl. Crystallogr.*, 2012, **45**, 849–854.

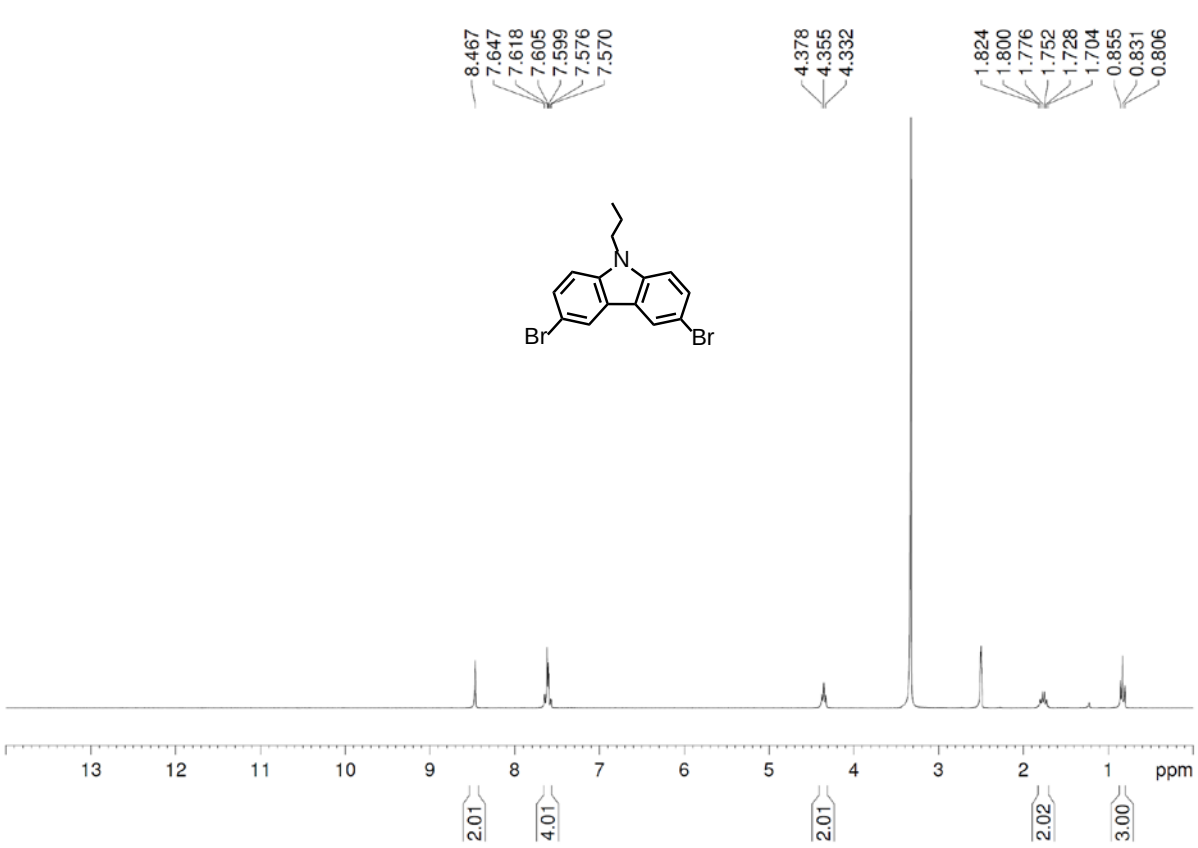


**Fig. S1** $^{1}$H NMR spectrum of 3,6-dibromo-9-*n*-propyl-9*H*-carbazole (DMSO-$d_6$).

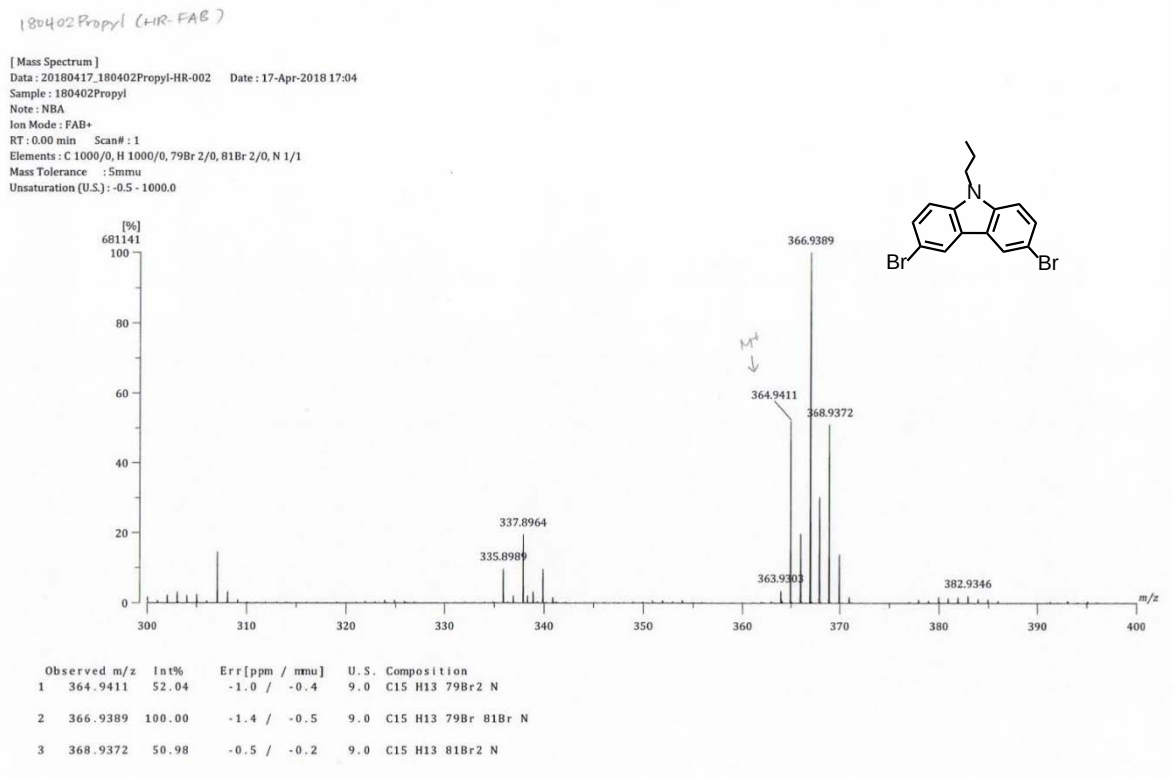


**Fig. S2** HR FAB-MS mass spectrum of 3,6-dibromo-9-*n*-propyl-9*H*-carbazole.

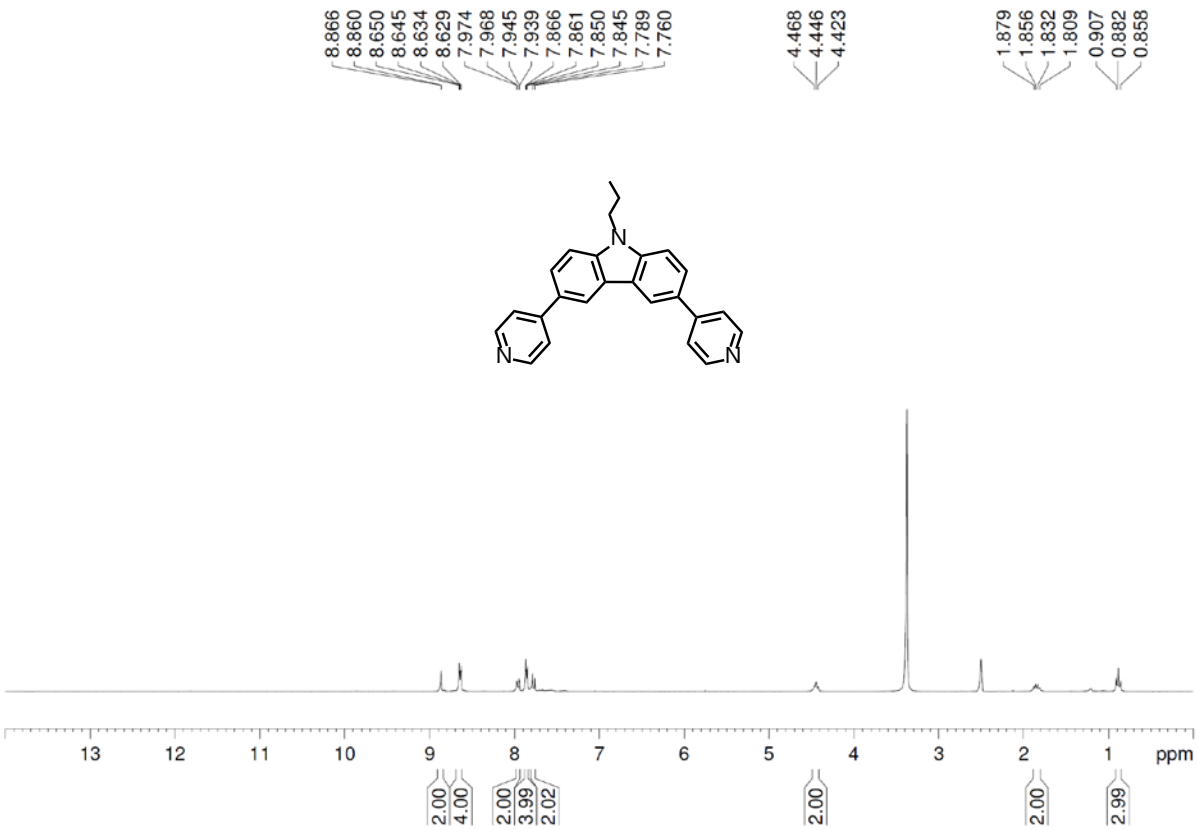


**Fig. S3** $^{1}$H NMR spectrum of Cz-Pr-3,6-bpy (DMSO-$d_6$).

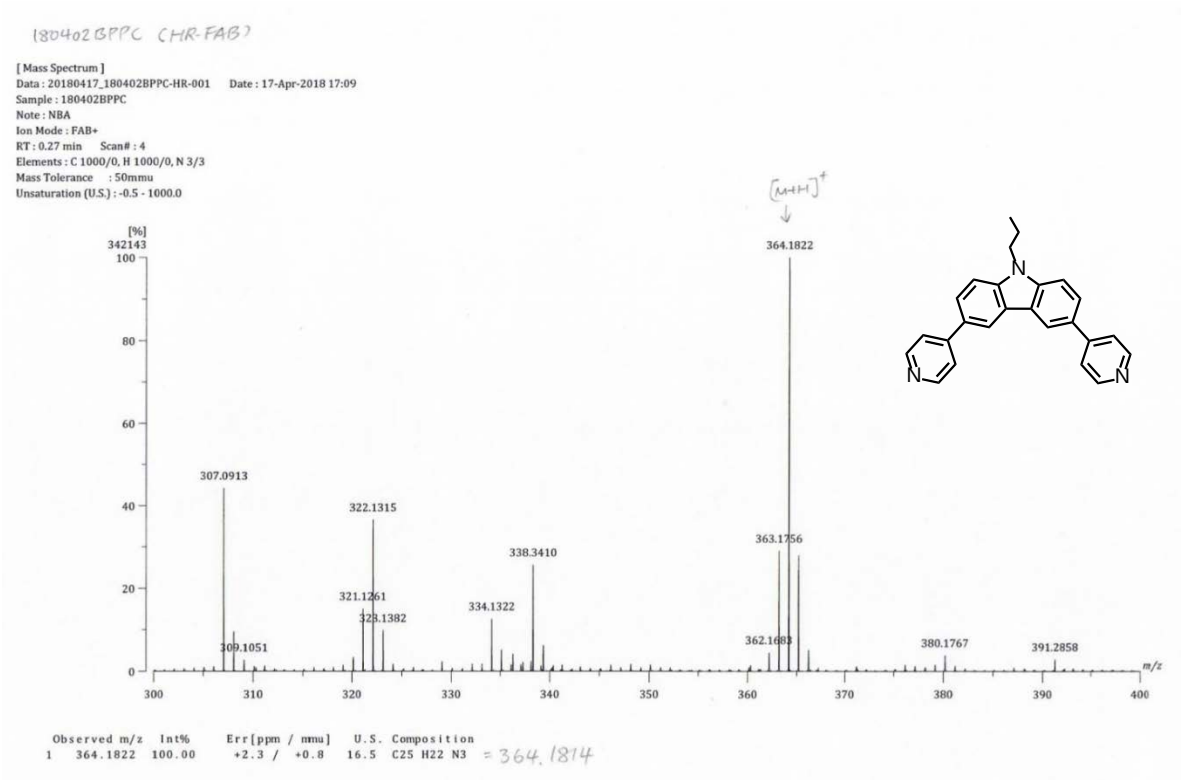


**Fig. S4** HR FAB-MS mass spectrum of Cz-Pr-3,6-bpy.

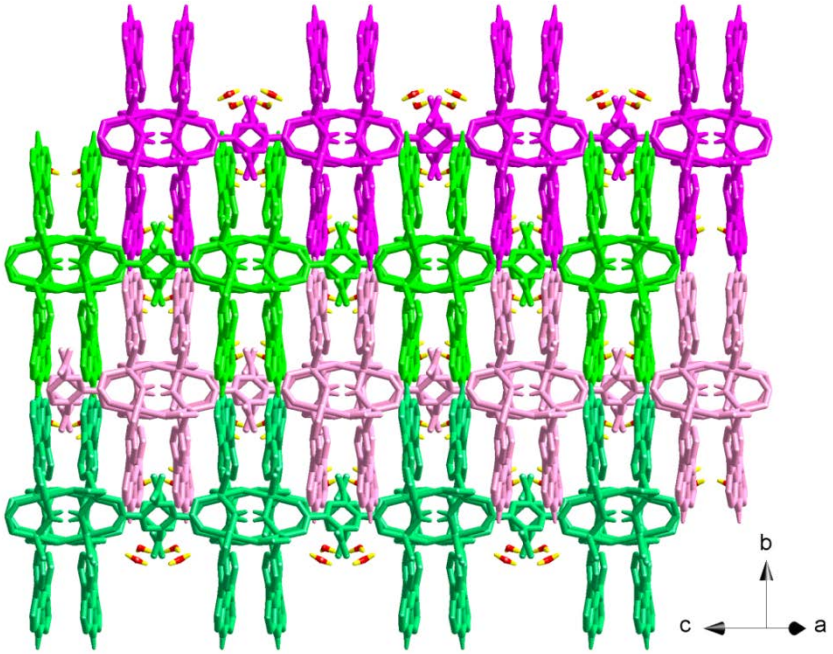


**Fig. S5** Packing diagram of **1**, showing these layers are intercalated each other along crystallographic [010] direction.

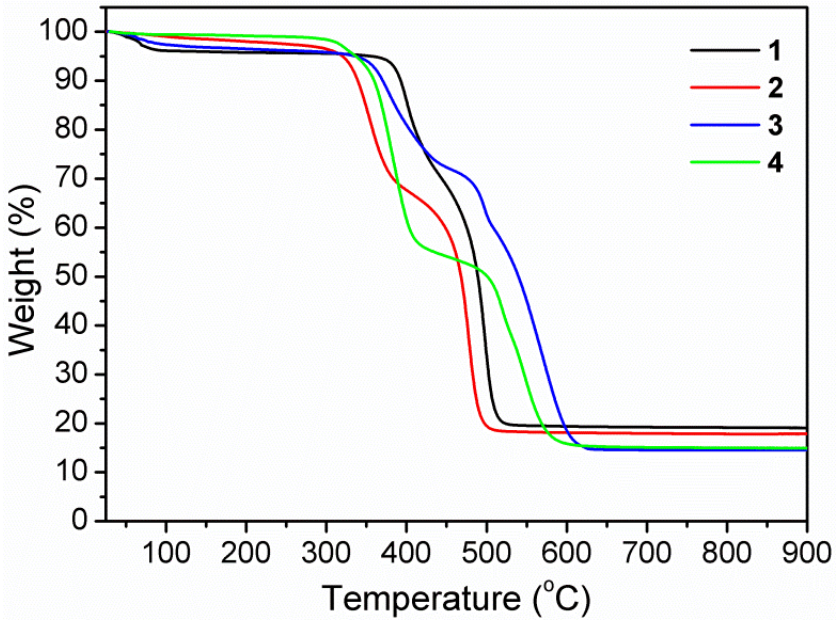


**Fig. S6** TG diagrams of **1**–**4**.

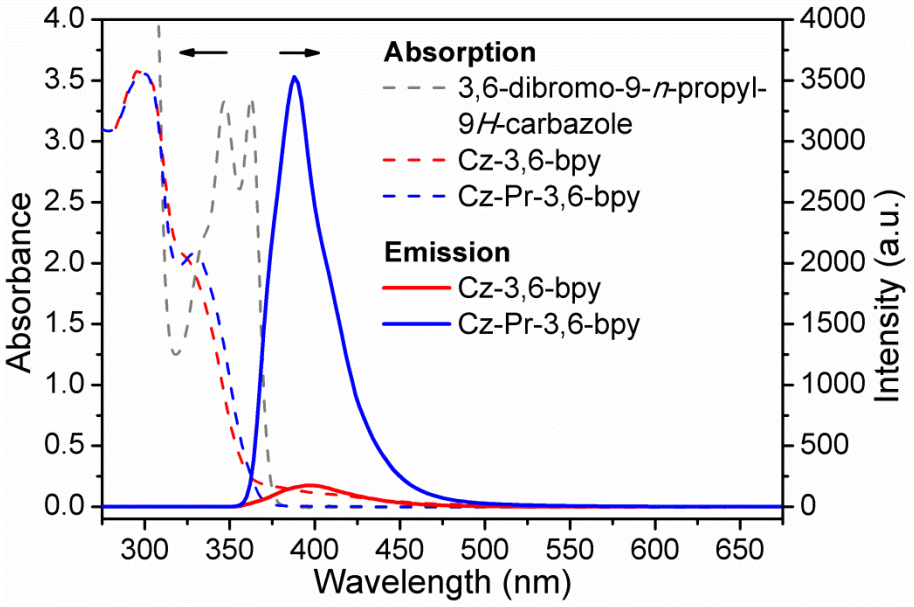


**Fig. S7** UV-Vis absorption spectra (dashed lines) of 3,6-dibromo-9-*n*-propyl-9*H*-carbazole, Cz-3,6-bpy, and Cz-Pr-3,6-bpy in DMF solution (0.1 mM) and photoluminescence spectra (solid lines) of Cz-3,6-bpy ($\lambda_{ex}$ = 360 nm) and Cz-Pr-3,6-bpy ($\lambda_{ex}$ = 365 nm) in DMF solution (1 mM).

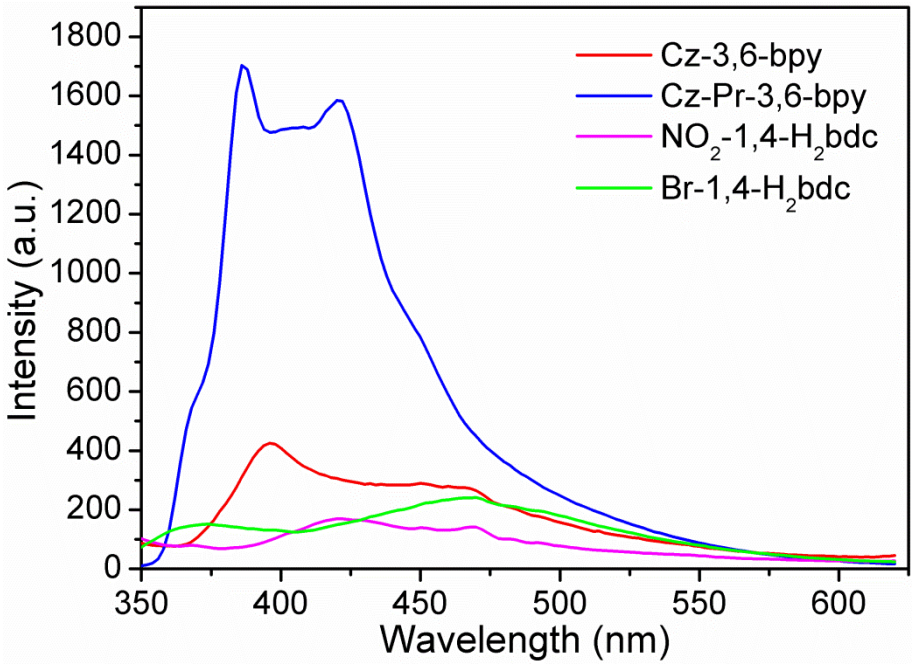


**Fig. S8** Room temperature solid-state emission spectra of Cz-3,6-bpy, Cz-Pr-3,6-bpy, $NO_2$-1,4-$H_2$bdc, and Br-1,4-$H_2$bdc upon excitation at $\lambda_{ex}$ = 320 nm.

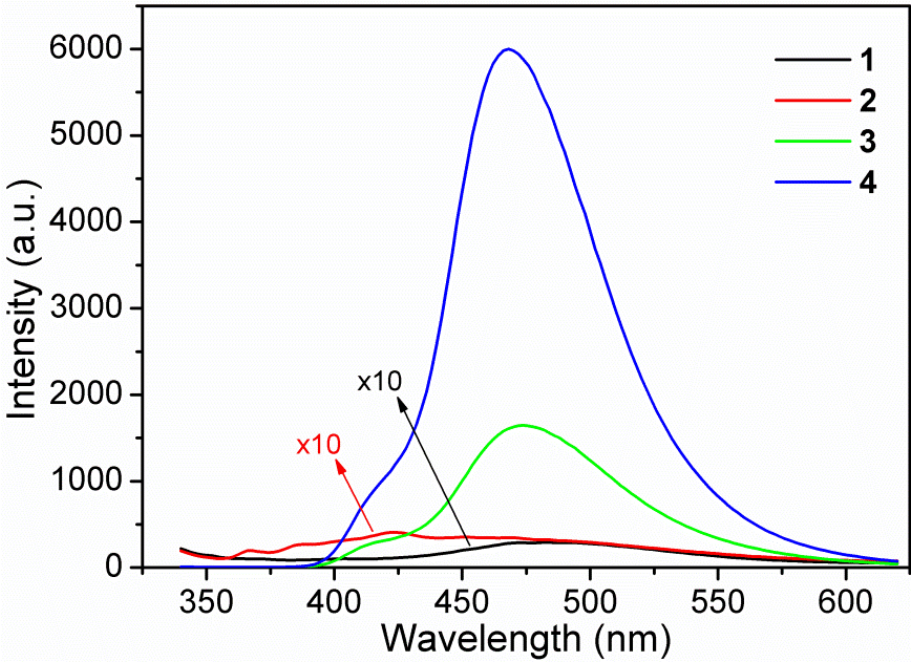


**Fig. S9** Room temperature solid-state emission spectra of **1**–**4** upon excitation at $\lambda_{ex}$ = 320 nm.

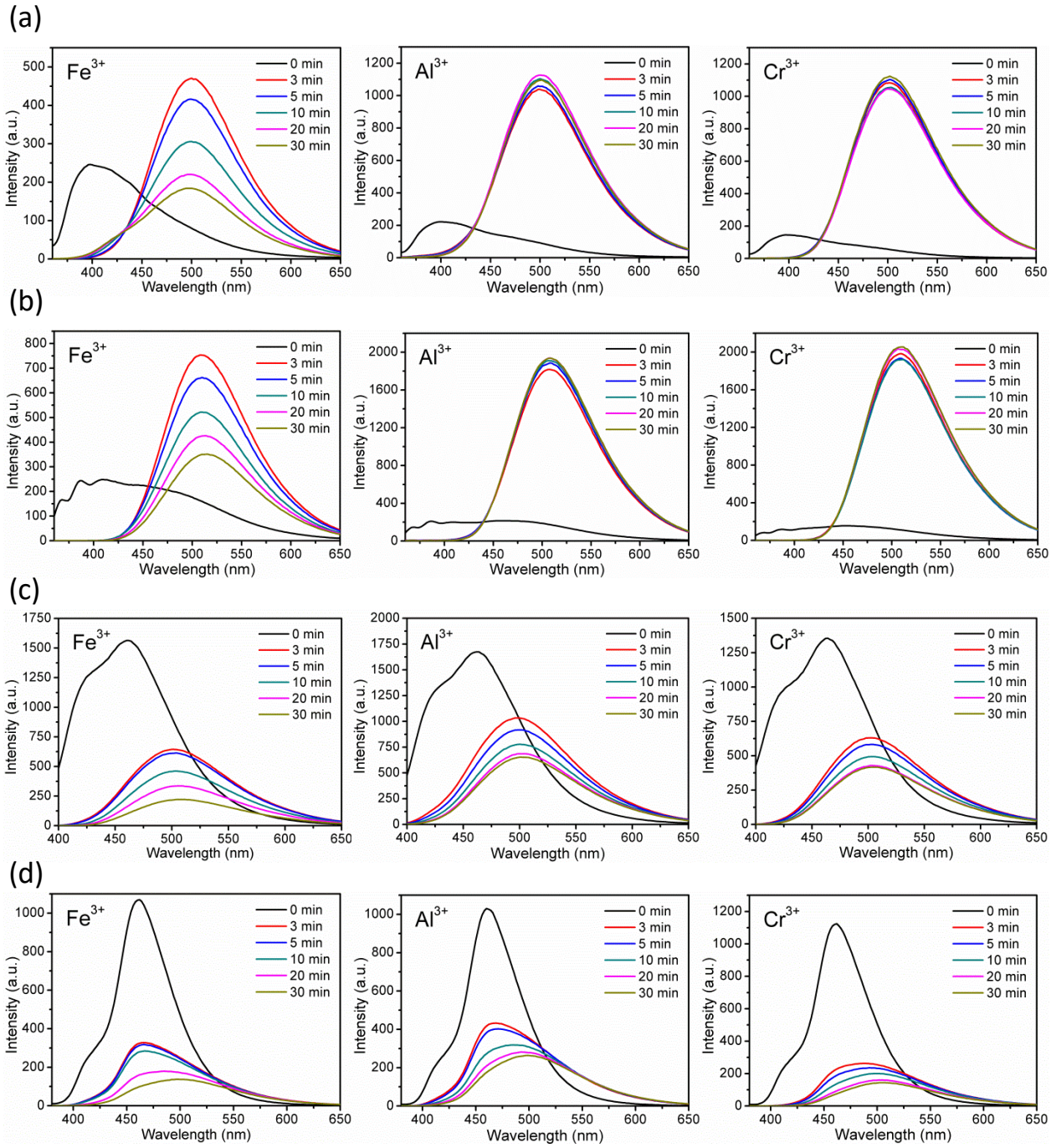


**Fig. S10** Time-dependent emission spectra of (a–d) **1**–**4** in sensing $Fe^{3+}$, $Al^{3+}$, and $Cr^{3+}$ in $H_2O$.

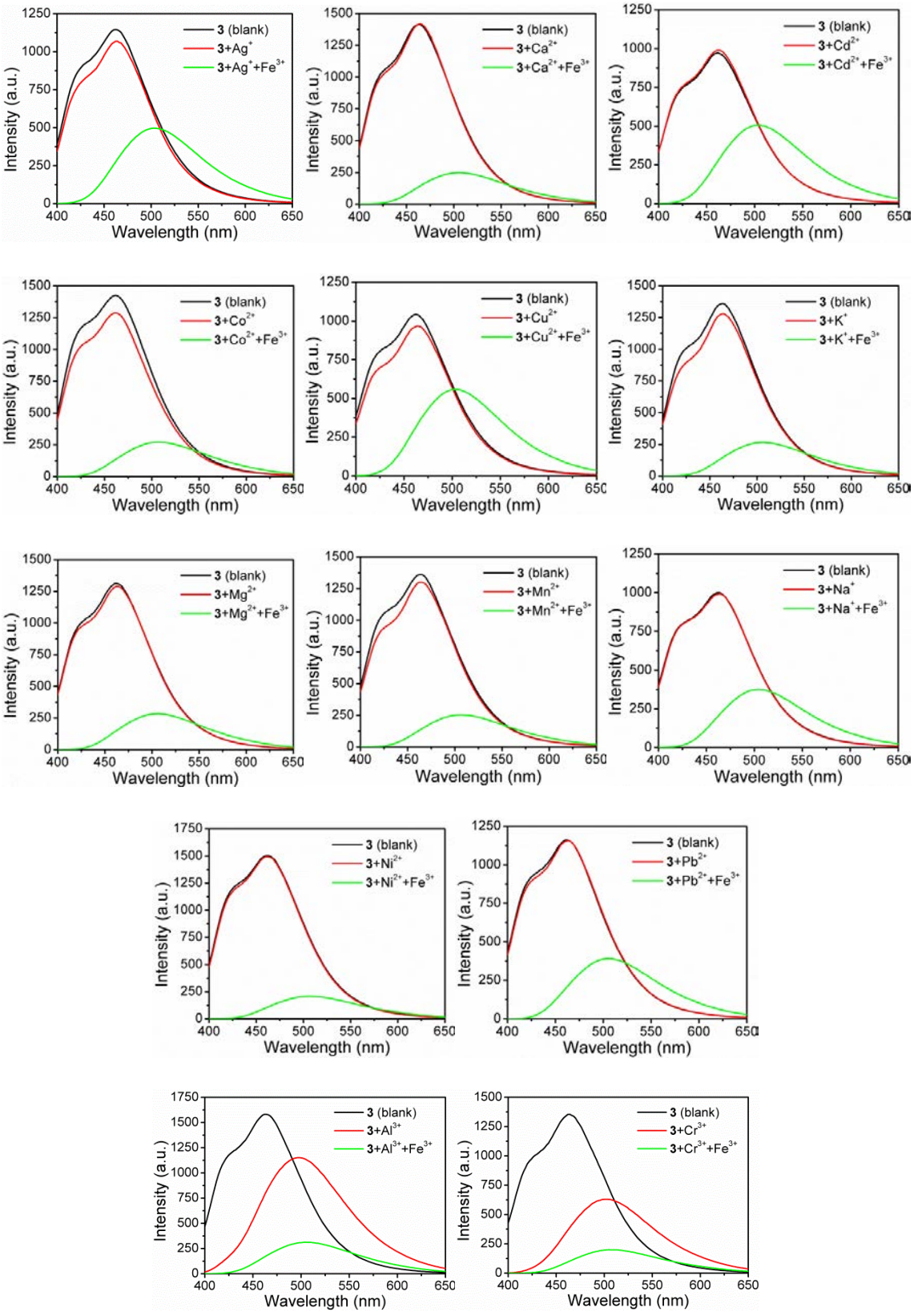


**Fig. S11** Emission spectra of **3** in $H_2O$ before and after addition of different perturbed metal ions, followed by the addition of $Fe^{3+}$ ions in equal concentration (1.0 mM).

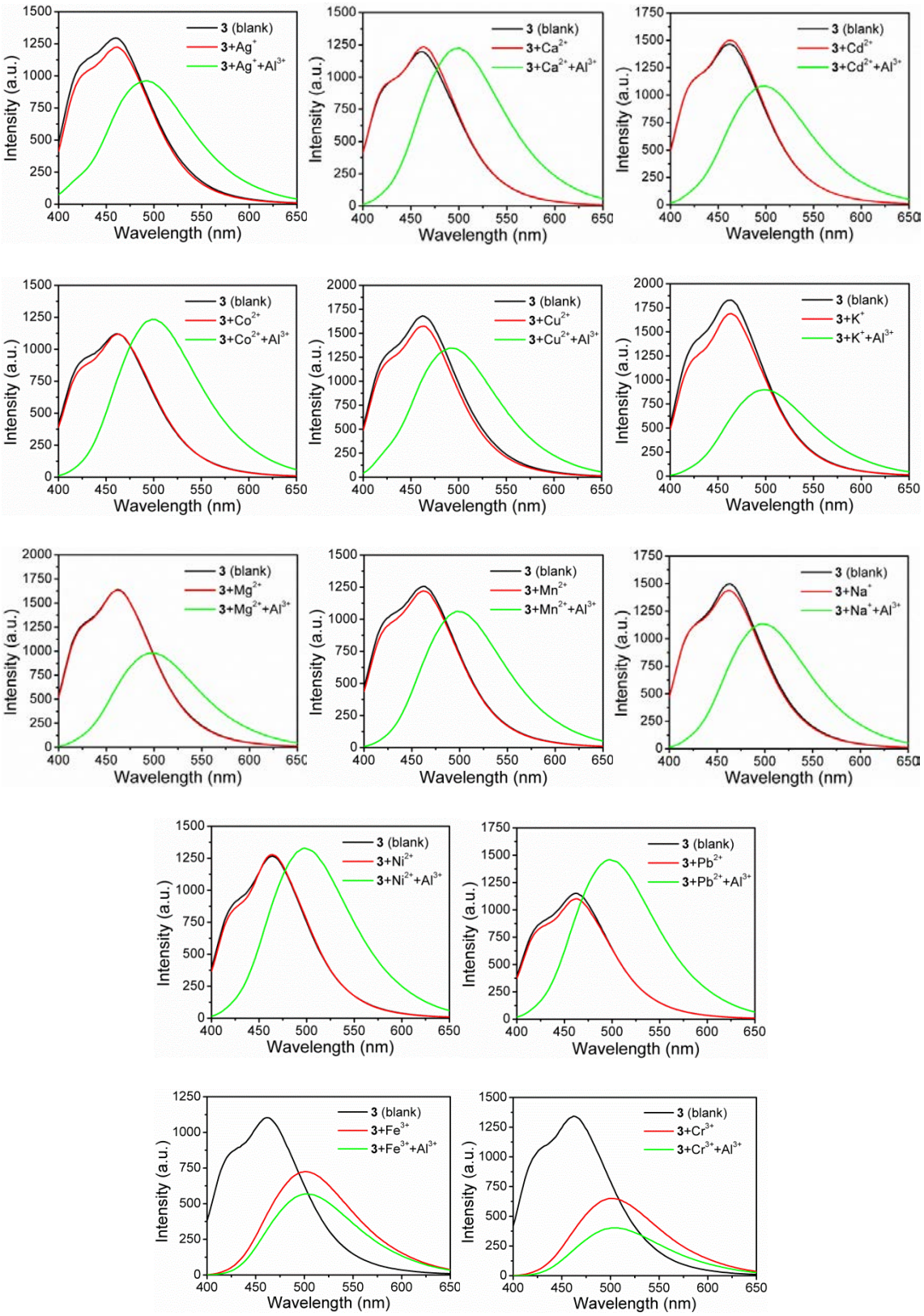


**Fig. S12** Emission spectra of **3** in $H_2O$ before and after addition of different perturbed metal ions, followed by the addition of $Al^{3+}$ ions in equal concentration (1.0 mM).

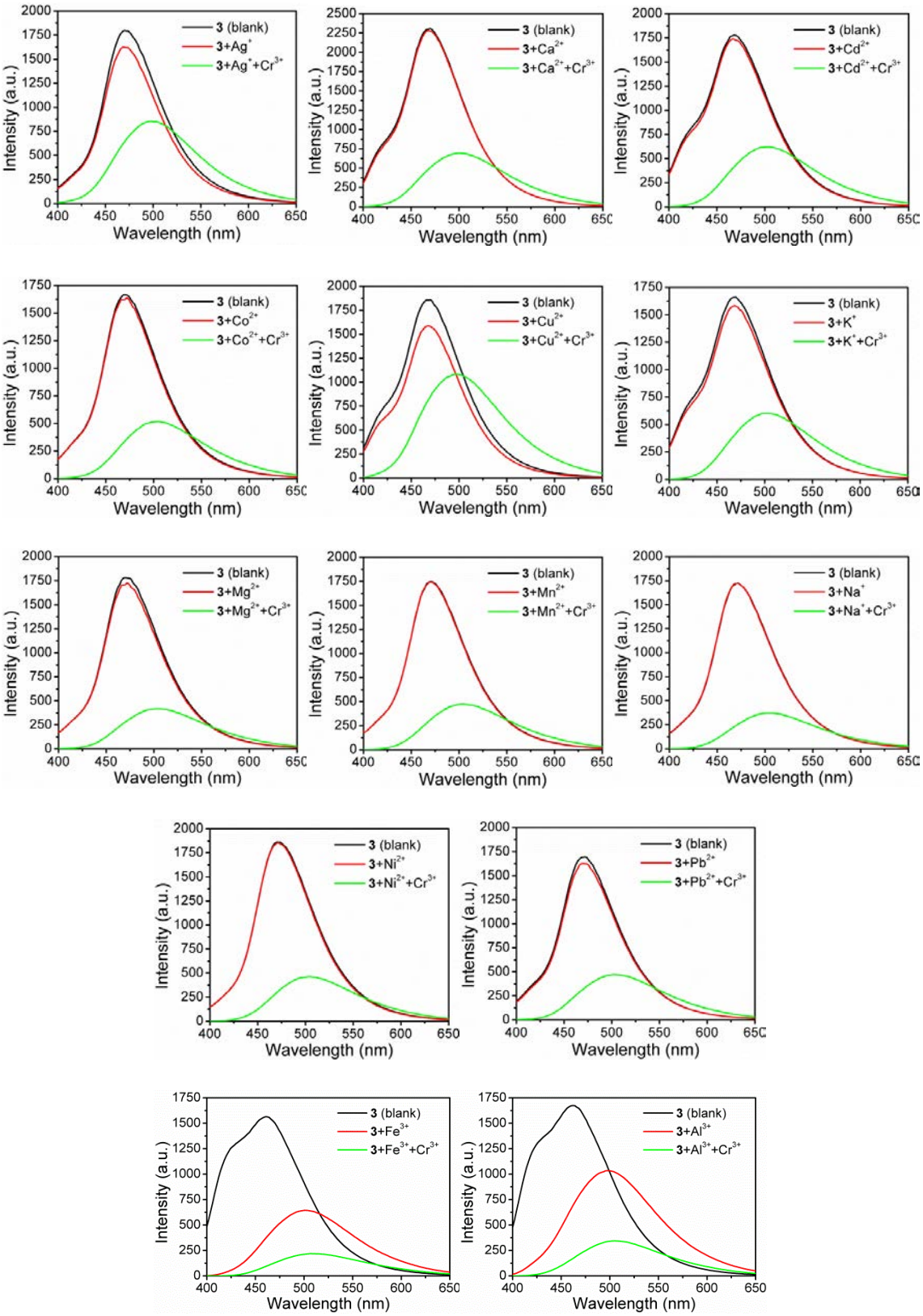


**Fig. S13** Emission spectra of **3** in $H_2O$ before and after addition of different perturbed metal ions, followed by the addition of $Cr^{3+}$ ions in equal concentration (1.0 mM).

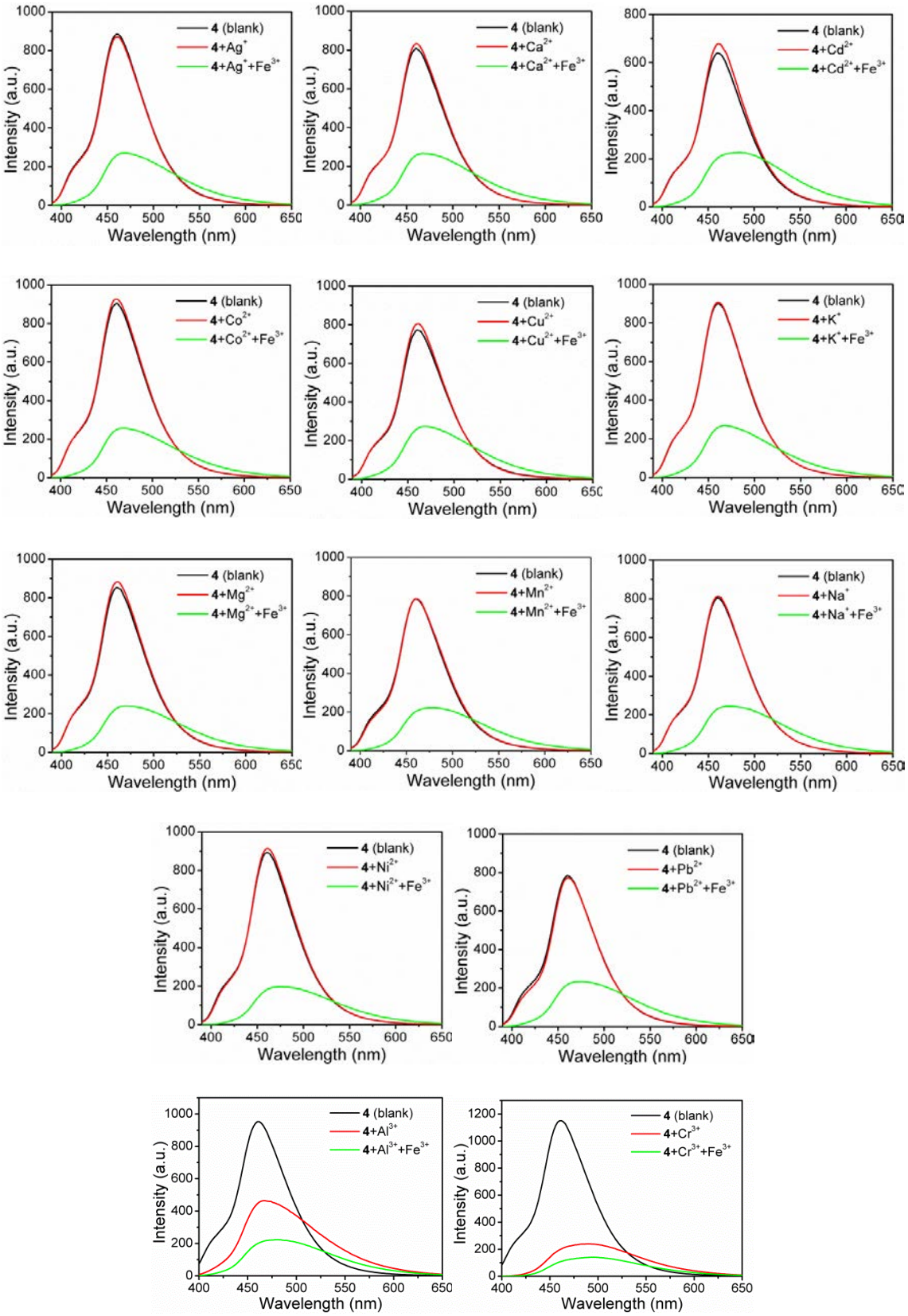


**Fig. S14** Emission spectra of **4** in $H_2O$ before and after addition of different perturbed metal ions, followed by the addition of $Fe^{3+}$ ions in equal concentration (1.0 mM).

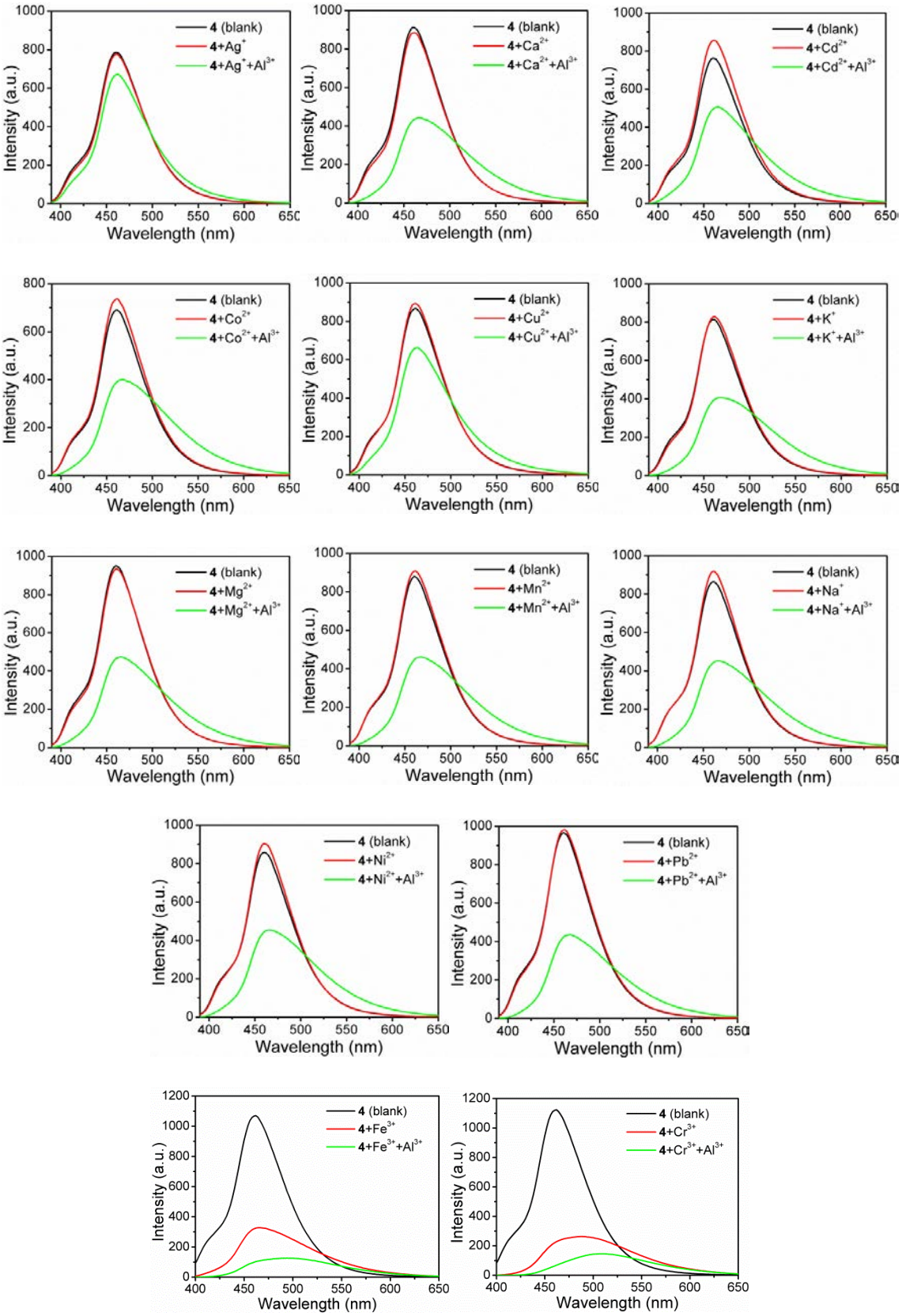


**Fig. S15** Emission spectra of **4** in $H_2O$ before and after addition of different perturbed metal ions, followed by the addition of $Al^{3+}$ ions in equal concentration (1.0 mM).

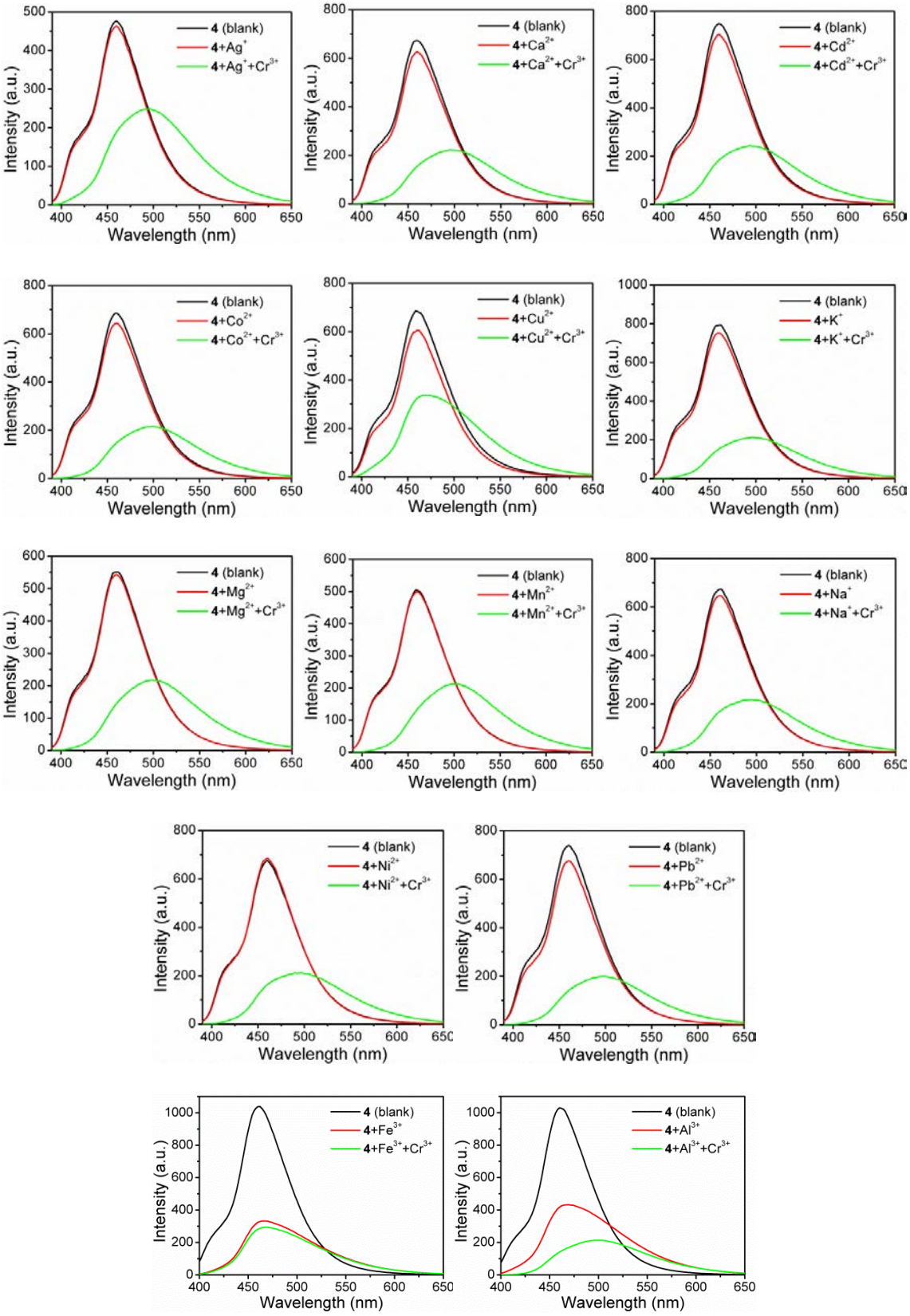


**Fig. S16** Emission spectra of **4** in $H_2O$ before and after addition of different perturbed metal ions, followed by the addition of $Cr^{3+}$ ions in equal concentration (1.0 mM).

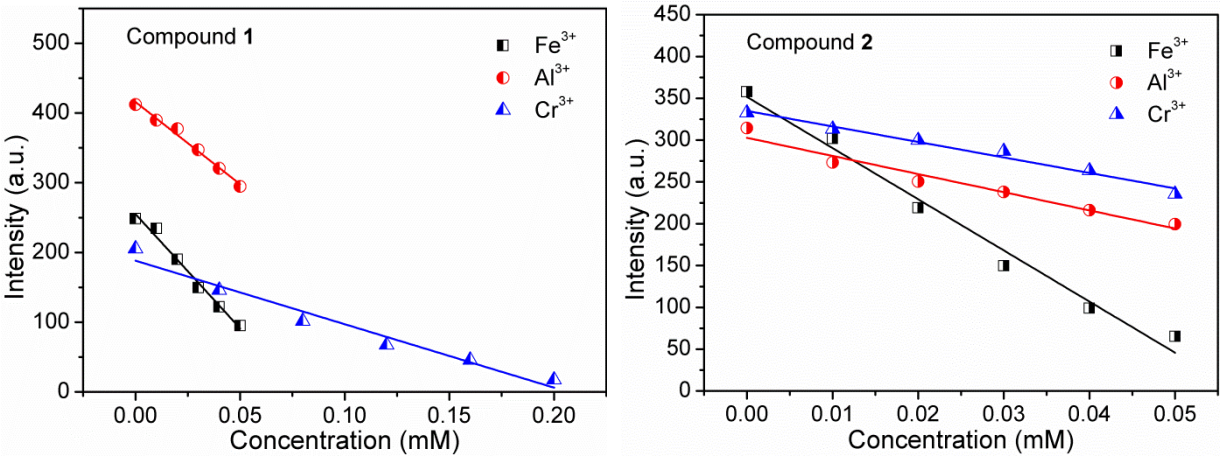


| | 1 | | | 2 | | |
|---|---|---|---|---|---|---|
| | $Fe^{3+}$ | $Al^{3+}$ | $Cr^{3+}$ | $Fe^{3+}$ | $Al^{3+}$ | $Cr^{3+}$ |
| Blank reading #1 | 241.7 | 414.6 | 205.5 | 357.5 | 304.8 | 330.5 |
| Blank reading #2 | 250.7 | 405.1 | 205.1 | 352.7 | 305.1 | 334.2 |
| Blank reading #3 | 247.9 | 408.1 | 207.4 | 351.9 | 310.2 | 335.8 |
| Blank reading #4 | 248.8 | 411.7 | 206.2 | 357.9 | 312.1 | 332.5 |
| Blank reading #5 | 248.7 | 412.1 | 205.4 | 357.8 | 314.4 | 332.6 |
| **Standard deviation (σ)** | 3.43 | 3.73 | 0.92 | 2.99 | 4.26 | 1.99 |
| **\| Slope (m) \|** | 3276 | 2359.1 | 911.1 | 6115.4 | 2167.1 | 1852.9 |
| $R^2$ | 0.98255 | 0.98576 | 0.95894 | 0.97999 | 0.95516 | 0.97403 |
| **LOD (3σ/m)** | **3.14 μM** | **4.74 μM** | **3.03 μM** | **1.47 μM** | **5.90 μM** | **3.22 μM** |

**Fig. S17** Linear region of fluorescence intensity for the $H_2O$ suspensions of **1** ($I$ = 412 nm for $Fe^{3+}$, 398 nm for $Al^{3+}$, 414 nm for $Cr^{3+}$) and **2** ($I$ = 386 nm) upon incremental addition of $Fe^{3+}$, $Al^{3+}$, and $Cr^{3+}$ ions. The following table lists the relevant parameters of LOD for the $H_2O$ suspensions of **1** and **2** toward $Fe^{3+}$, $Al^{3+}$, and $Cr^{3+}$ ions.

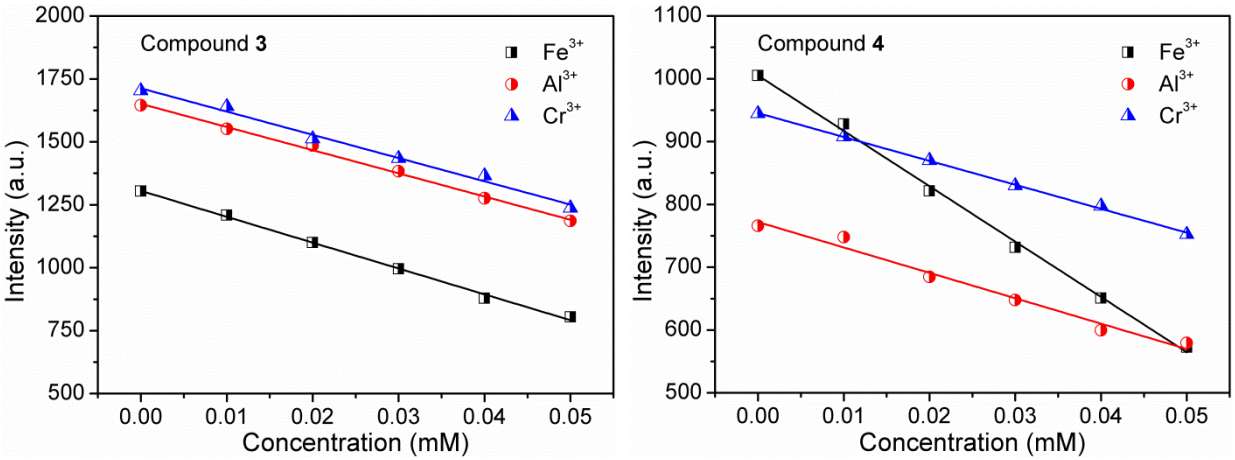


| | 3 | | | 4 | | |
|---|---|---|---|---|---|---|
| | $Fe^{3+}$ | $Al^{3+}$ | $Cr^{3+}$ | $Fe^{3+}$ | $Al^{3+}$ | $Cr^{3+}$ |
| Blank reading #1 | 1307 | 1647 | 1701 | 1005 | 766.2 | 944.7 |
| Blank reading #2 | 1311 | 1650 | 1700 | 1009 | 772.2 | 944.8 |
| Blank reading #3 | 1312 | 1647 | 1700 | 1011 | 766.8 | 939.2 |
| Blank reading #4 | 1310 | 1648 | 1699 | 1007 | 768.4 | 940 |
| Blank reading #5 | 1304 | 1645 | 1703 | 1005 | 766.1 | 944.3 |
| **Standard deviation (σ)** | 3.27 | 1.82 | 1.52 | 2.61 | 2.55 | 2.76 |
| **\| Slope (m) \|** | 10274.3 | 9205.7 | 9237.1 | 8808 | 4044.9 | 3804.9 |
| $R^2$ | 0.9969 | 0.99528 | 0.98835 | 0.99697 | 0.97574 | 0.99861 |
| **LOD (3σ/m)** | **0.96 μM** | **0.59 μM** | **0.49 μM** | **0.89 μM** | **1.89 μM** | **2.18 μM** |

**Fig. S18** Linear region of fluorescence intensity for the $H_2O$ suspensions of **3** and **4** upon incremental addition of $Fe^{3+}$, $Al^{3+}$, and $Cr^{3+}$ ions. The following table lists the relevant parameters of LOD for the $H_2O$ suspensions of **3** and **4** toward $Fe^{3+}$, $Al^{3+}$, and $Cr^{3+}$ ions.

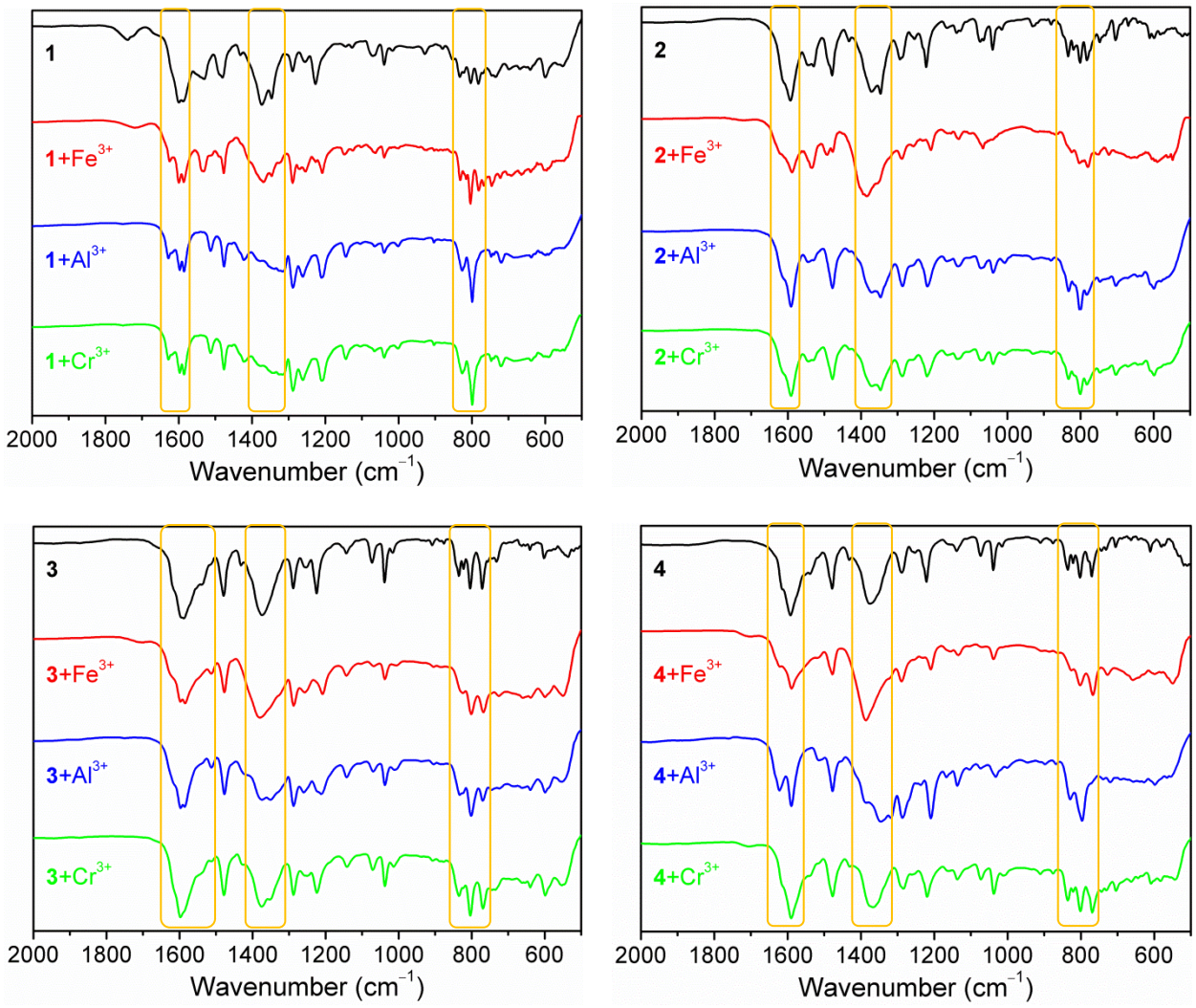


**Fig. S19** IR spectra of compounds **1**–**4** in the region of 2000–500 $cm^{-1}$ before and after treated with $Fe^{3+}$, $Al^{3+}$, and $Cr^{3+}$ ions.

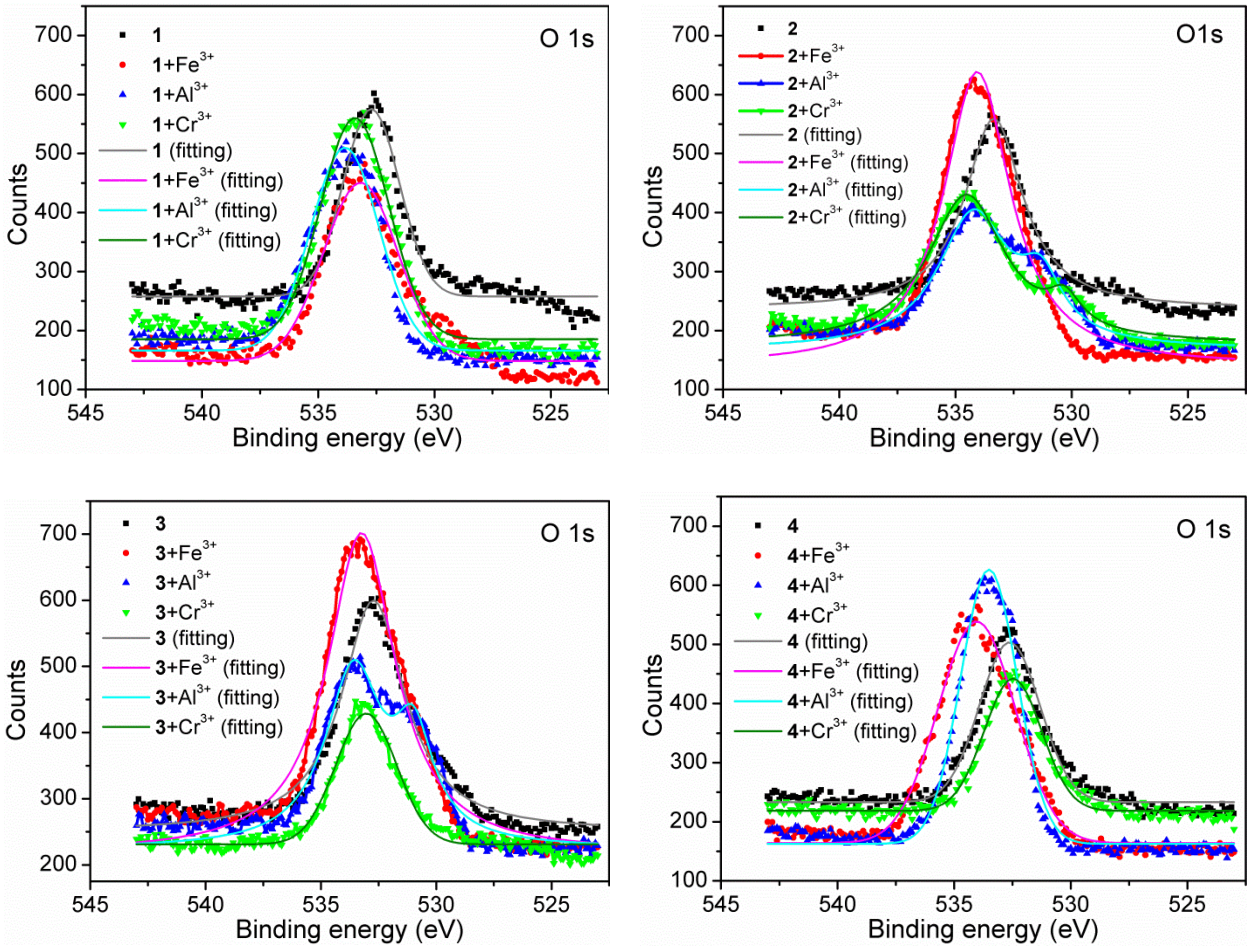


**Fig. S20** O 1s XPS spectra of compounds **1**–**4** before and after treated with $Fe^{3+}$, $Al^{3+}$, and $Cr^{3+}$ ions.

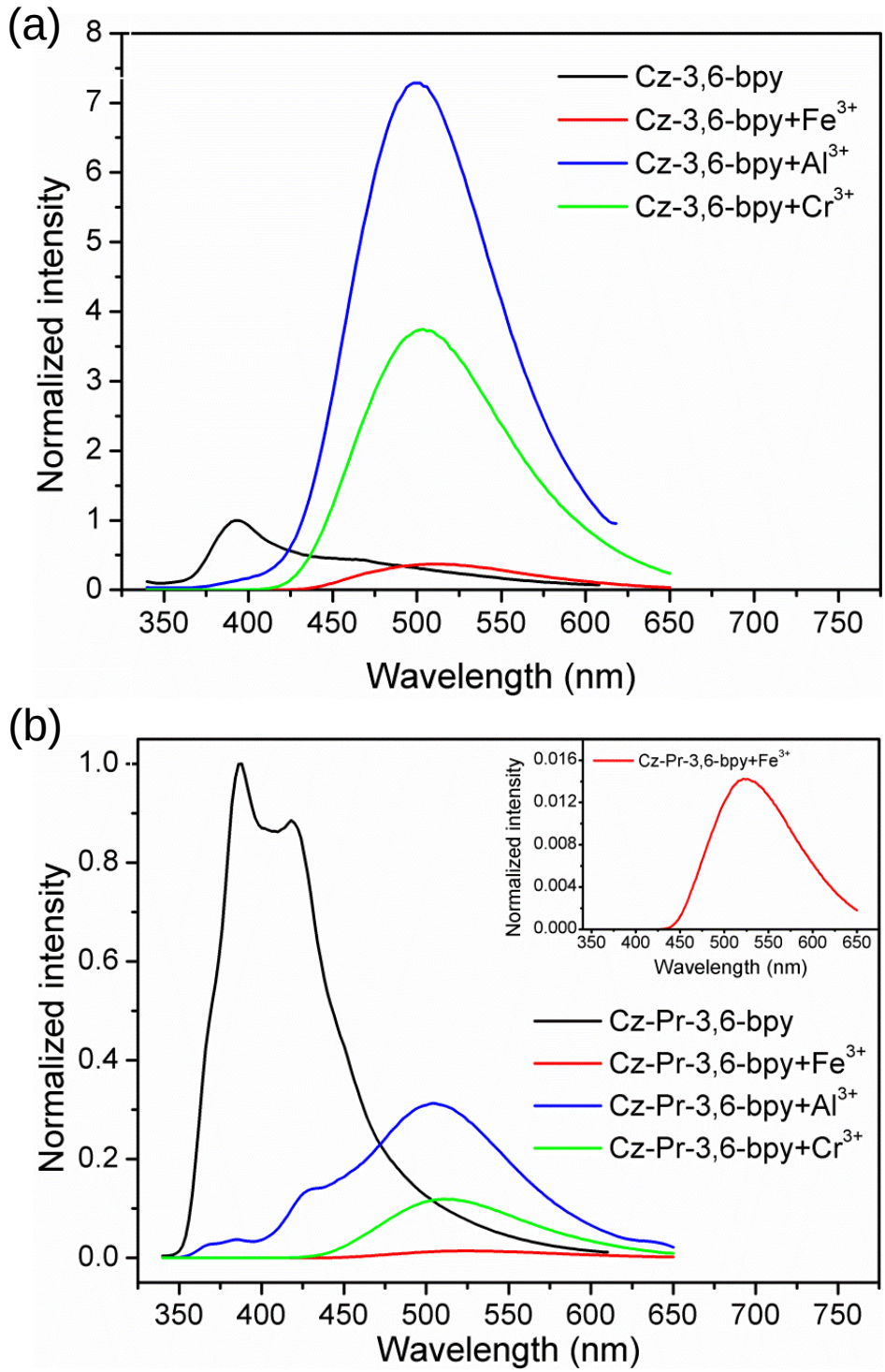


**Fig. S21** Normalized emission spectra of (a) Cz-3,6-bpy and (b) Cz-Pr-3,6-bpy in $H_2O$ suspensions (1 mg/3 mL) before and after addition of $Fe^{3+}$, $Al^{3+}$, and $Cr^{3+}$ ions (1.0 mM).

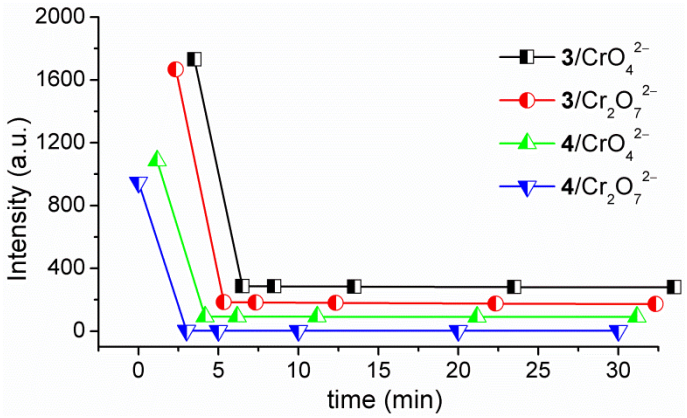


**Fig. S22** Time-dependent emission intensities of **1**–**4** in sensing $CrO_4^{2-}$ and $Cr_2O_7^{2-}$.

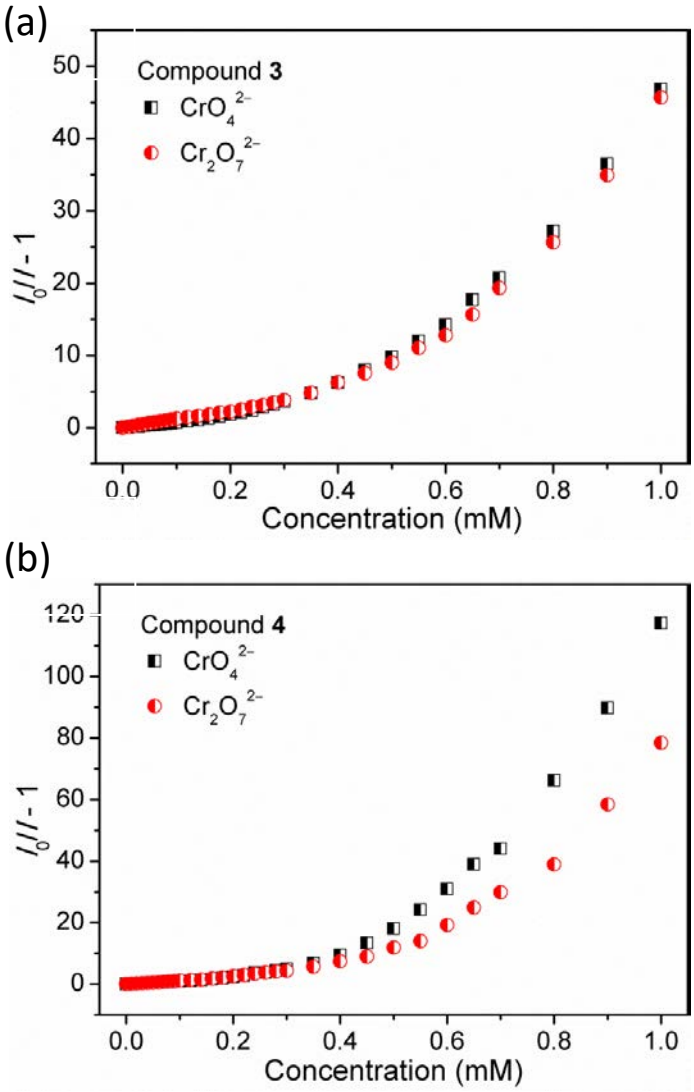


**Fig. S23** The Stern–Volmer plots of (a) **3** and (b) **4** for the detection of $CrO_4^{2-}$ and $Cr_2O_7^{2-}$ with different concentrations in the range 0–1.0 mM.

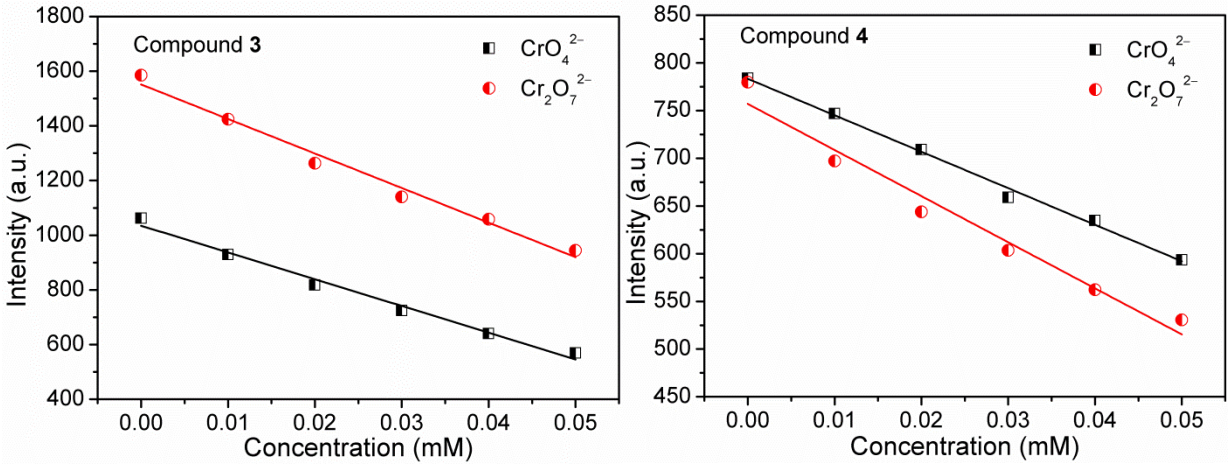


| | **3** | | **4** | |
|---|---|---|---|---|
| | $CrO_4^{2-}$ | $Cr_2O_7^{2-}$ | $CrO_4^{2-}$ | $Cr_2O_7^{2-}$ |
| Blank reading #1 | 1064 | 1581 | 783.4 | 781.8 |
| Blank reading #2 | 1059 | 1584 | 786.9 | 779.3 |
| Blank reading #3 | 1064 | 1585 | 783.4 | 780.1 |
| Blank reading #4 | 1057 | 1585 | 784.4 | 783.8 |
| Blank reading #5 | 1062 | 1585 | 783.8 | 780.5 |
| **Standard deviation (σ)** | 3.11 | 1.73 | 1.47 | 1.76 |
| **\| Slope (m) \|** | 9784 | 12630 | 3823.7 | 4831.7 |
| $R^2$ | 0.9846 | 0.98131 | 0.99407 | 0.96351 |
| **LOD (3σ/m)** | **0.96 μM** | **0.41 μM** | **1.15 μM** | **1.09 μM** |

**Fig. S24** Linear region of fluorescence intensity for the $H_2O$ suspensions of **3** and **4** upon incremental addition of $CrO_4^{2-}$ and $Cr_2O_7^{2-}$ ions. The following table lists the relevant parameters of LOD for the $H_2O$ suspensions of **3** and **4** toward $CrO_4^{2-}$ and $Cr_2O_7^{2-}$ ions.

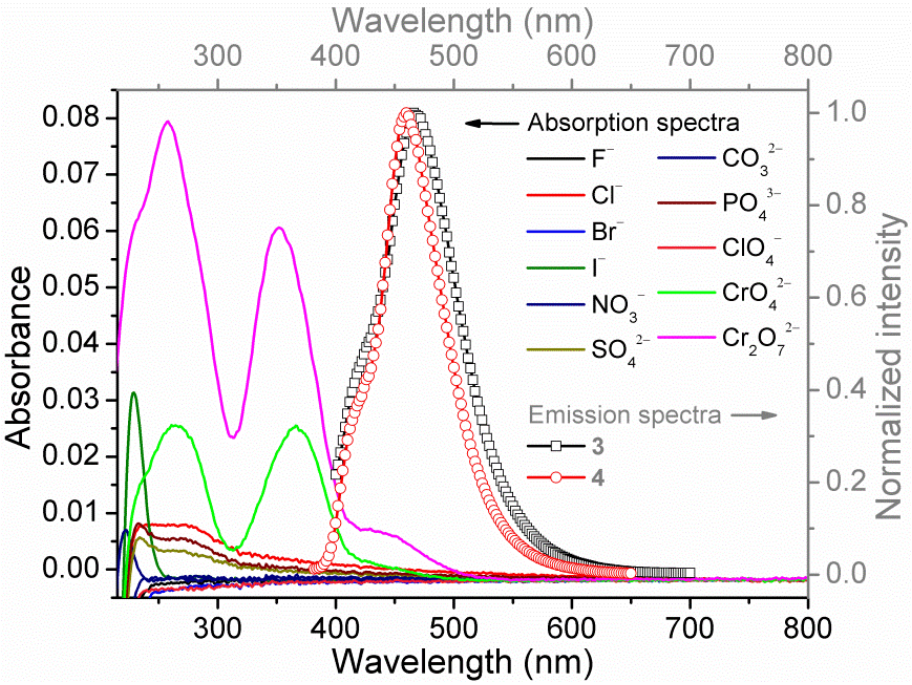


**Fig. S25** Overlapping of the UV-vis absorption spectra of anions in aqueous solutions and the normalized luminescent emission spectra of **3** and **4** in $H_2O$.